Supplementary Information (SI) for Journal of Materials Chemistry C.

Thermal driven morphology and lattice transfer of NiCo alloy for accelerating electrocatalytic water splitting

Qingyi Qian[a]; Lixia Li[a]; Jiamin Liu[a]; Xi Duo*[a]; Ruifang Yang[c]; Xiaowei Li[a]; Quanquan Shi[a]; Xingkai Zhang[b]; Bo Hai*[a]

[a] College of Science a & College of Material Science and Art Design, Inner Mongolia Agricultural University, Hohhot 010018, China.

[b] Key Laboratory of Science and Technology on Wear and Protection of Materials, Lanzhou Institute of Chemical Physics, Chinese Academy of Sciences, Lanzhou 730000, China.

[c] Management Center of Laboratory and Equipment, Inner Mongolia Agricultural University, Hohhot 010018, China.

(1) Carrier pretreatment

The 2cm × 4.5cm copper sheet in 3 M HCl for 2min to remove the surface oxides, and use deionized water and ethanol to remove the residual HCl on the surface, and finally, use nitrogen to blow dry the copper sheet and set aside.

(2) Preparation of metal films

Co base solution configuration

The 0.15 g of $CoCl_2 \cdot 6\ H_2O$ and 3 g of a NH_4Cl into 100 ml of deionized water and stirred magnetically for 5min to mix it well.

Preparation of an amorphous Co films

The cleaning Cu sheet was used as the working electrode, a carbon rod as the counter electrode, and an Ag/AgCl electrode as the reference electrode. Plating was applied in the above configured solution. Electrodeposition was carried out at a constant current of 100 mA cm^{-2} for 200 s to obtain Ni film, Co film and Ni, Co alloy films with different molar ratios. The samples were rinsed with deionized water and ethanol, respectively, and blown dry with nitrogen to be prepared for testing.

Preparation of metal Ni films.

The 0.15 g of $NiCl_2 \cdot 6\ H_2O$ and 3 g of a NH_4Cl into 100 ml of deionized water and stirred magnetically for 5min to mix it well.

The same electrodeposition method was used to prepare the mental Ni films.

Ni-Co alloy films with different nickel-cobalt ratios

The 0.75 g of $CoCl_2 \cdot 6\ H_2O$ and 0.75 g of $NiCl_2 \cdot 6\ H_2O$ were dissolved into 100 ml deionized water with 3 g NH_4Cl adding. The solution was stirred magnetically enough for 5 min to mix it well. The different Ni and Co metal salt ratio content solution were changed by adding in $CoCl_2 \cdot 6\ H_2O$ and $NiCl_2 \cdot 6\ H_2O$ ratio content to gain. The $CoCl_2 \cdot 6\ H_2O$ was 0.05 g and 0.6 g, respectively. The $NiCl_2 \cdot 6\ H_2O$ was 0.1 g and 0.9 g, respectively. The NiCo alloy ratio content was 1:1, 1.5:1 and 2:1, respectively.

The same electrodeposition method was used to prepare the Nico-cobalt alloy membrance.

2.4 Electrochemical test

All the electrochemical measurements were collected by CHI760E electrochemical workstation (Shanghai Chenhua Co.). Electrochemical performances of all the samples were carried out with a standard three-electrode system in 1.0 M KOH. In which, carbon rods and Ag/AgCl electrode were employed counter electrode and reference electrode. The sample as working electrode (1cm×1cm), respectively. All the potentials involved in this work have been referenced to reversible hydrogen electrode (RHE) with the Nernst equation: $E_{(RHE)} = E_{(Ag/AgCl)} + 0.197\ V + 0.0592 \times pH$.

For the HER measurements, the linear sweep voltammetry (LSV) curves were executed at the potential range between -0.5 to -1.5 V *vs.* Ag/AgCl with a scan rate of 5 mV s^{-1}. The overpotential (η) was calculated with the following equation: $\eta = E_{(\mathrm{RHE})} - 0$ V. The potentials were referenced by *iR* correction = 90%. The electrochemical impedance spectroscopy (EIS) plots were collected at the potential of –10 mA cm^{-2} (E10) with frequency range from 100 kHz to 0.01 Hz, Catalyst stability was determined using i-t curves at 10 mA cm^{-2} process potential.

The OER activities were measured using the linear voltammetry (LSV) technique. LSV curves were executed at the potential range between 0 to 1 V vs. Ag/AgCl with a scan rate of 5 mV s^{-1}. And then, the potentials were referenced by iR correction=90%. The overpotential (η) was calculated with the following equation: $\eta = E_{(\mathrm{RHE})} - 1.23$ V. The electrochemical impedance spectroscopy (EIS) plots were collected at the potential of 0.5 V with a frequency range from 100 kHz to 0.01 Hz. Electrochemical surface area (ECSA) testing by cyclic voltammetry. Catalyst stability was determined using i-t curves at 20 mA cm^{-2} process potential.

The loading Ni and Co content was detected by inductively coupled plasma optical emission spectroscopy (Agilent ICP-OES 5800)

Description of data calculations:

$$Cx\left(\frac{mg}{Kg}\right) = \frac{C_0\left(\frac{mg}{L}\right) * f * v_0(ml) * 10^{-3}}{m(g) * 10^{-3}} = \frac{C_1\left(\frac{mg}{L}\right) * f * v_0(ml) * 10^{-3}}{m(g) * 10^{-3}}$$

$$w(\%) = \frac{C_x(\frac{mg}{Kg})}{10^6} * 100\%$$

$$C_1\left(\frac{mg}{L}\right) = C_0\left(\frac{mg}{L}\right) * f$$

m_0: the mass in grams (g) of the sample taken when analyzing the sample, which is recorded by the analytical balance.

V_0: volume in milliliters (mL) of the sample after elimination and volume of the sample to be fixed.

C_o: Concentration of the element in the test solution in milligrams per liter (mg/L).

C_1: Elemental concentration in milligrams per liter (mg/L) of the sample abatement solution stock.

C_x: Final test result for the element measured, in milligrams per kilogram (mg/kg).

Computational Methods

Spin-polarized First-principle calculations were performed by the density functional theory (DFT) using the Vienna Ab-initio Simulation Package (VASP) package [1]. The generalized gradient approximation (GGA) with the Perdew-Burke-Ernzerhof (PBE) functional were used to describe the electronic exchange and correlation effects [2,3,4]. Uniform G-centered k-points meshes with a resolution of

$2\pi*0.04$ Å^{-1} and Methfessel-Paxton electronic smearing were adopted for the integration in the Brillouin zone for geometric optimization. The simulation was run with a cutoff energy of 500 eV throughout the computations. These settings ensure convergence of the total energies to within 1 meV per atom. Structure relaxation proceeded until all forces on atoms were less than 1 meV Å^{-1} and the total stress tensor was within 0.01 GPa of the target value.

The free energy of the adsorption atomic hydrogen (ΔG_{H*}) is obtained by

$$\Delta G_{H*} = \Delta E_{H*} + \Delta E_{ZPE} - T\Delta S_{H*}$$

ΔE_{H*} describes the energy needed to increase the coverage by one hydrogen atom. ΔE_{ZPE} is the difference in zero point energy and ΔS_{H*} is the difference in entropy. $\Delta E_{ZPE} - T\Delta S_{H*}$ is about 0.24 eV, so $\Delta G_{H*} = \Delta E_{H*} + 0.24$ [5]. For ΔE_{H*}, it is calculated as follows:

$$\Delta E_{H*} = E(\text{surface+H}) - E(\text{surface}) - 1/2\ E(H_2)$$

Where E(surface+H) represents the total energy of the selected surfaces with one adsorbed hydrogen atom on the surfaces, E(surface) represents the total energy of the surfaces, while $E(H_2)$ represents the total energy of a gas phase H_2 molecule.

Generally, in alkaline media, the OER reaction mechanism can be written as 4-elecetron change mechanism:

Step1: $* + OH^- \rightarrow OH* + e^-$

Step2: $OH* + OH^- \rightarrow O* + H_2O + e^-$

Step3：$O* + OH^- \rightarrow OOH* + e^-$

Step4：$OOH* + OH^- \rightarrow O_2\ (g) + * + H_2O + e^-$

where * presents an adsorption site on the catalyst, and OH*, O*, and OOH* denotes the corresponding absorbed intermediates. The theoretical overpotential η for OER can be calculated using the equations:

$$G^{OER} = \max\ \{\Delta G1, \Delta G2, \Delta G3, \Delta G4\}$$

$$\eta^{OER} = G_{OER}/e - 1.23\ V$$

Supplementary Figures

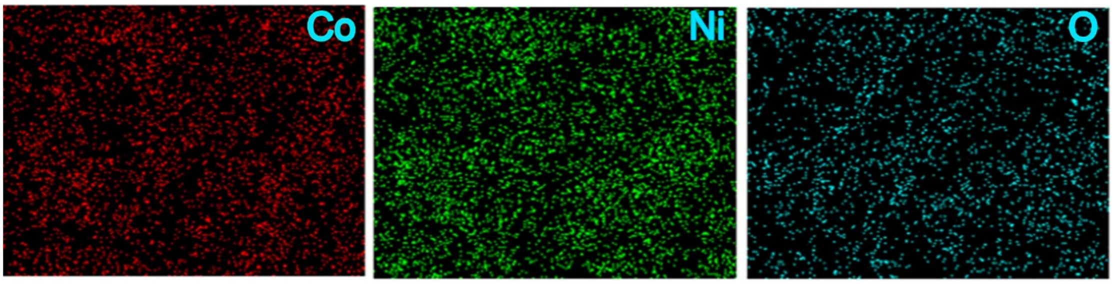

Fig. S1 Element distribution of Ni:Co=1.5:1 alloys

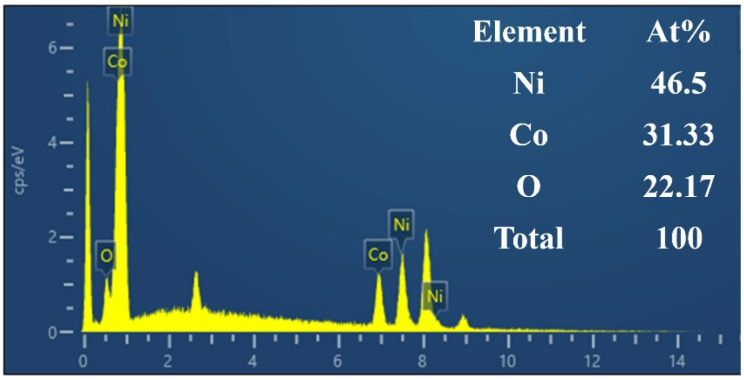

Element	At%
Ni	46.5
Co	31.33
O	22.17
Total	100

Fig. S2 Element content of Ni:Co=1.5:1 alloys

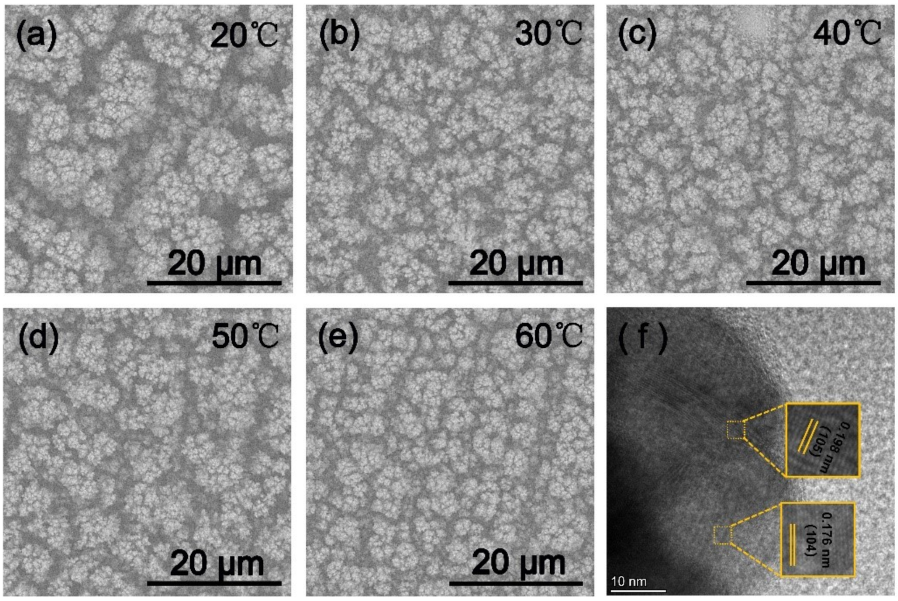

Fig. S3 a-e) are SEM images of Ni:Co=1.5:1 catalyst after 3 HER tests at different temperatures, and f) is a TEM image after 8 h HER stability.

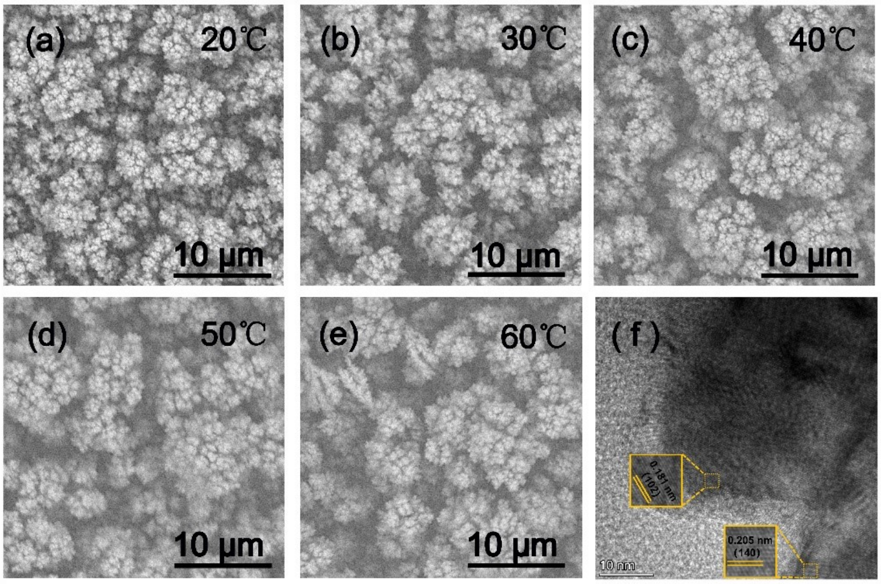

Fig. S4 a-e) are SEM images of Ni:Co=1.5:1 catalyst after 3 OER tests at different temperatures, and f) is a TEM image after 8 h OER stability.

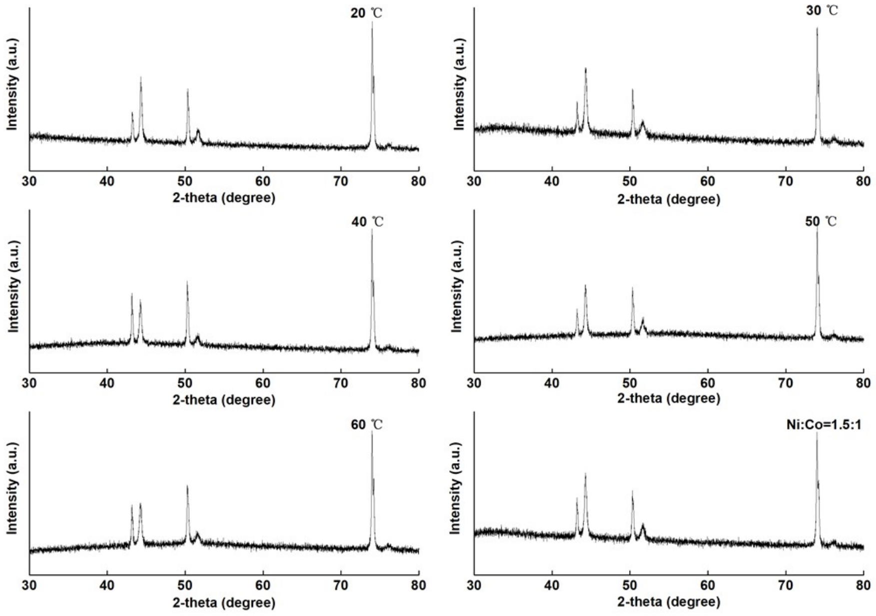

Fig. S5 shows the XRD images of the Ni:Co=1.5:1 catalyst after three LSV tests at different temperatures.

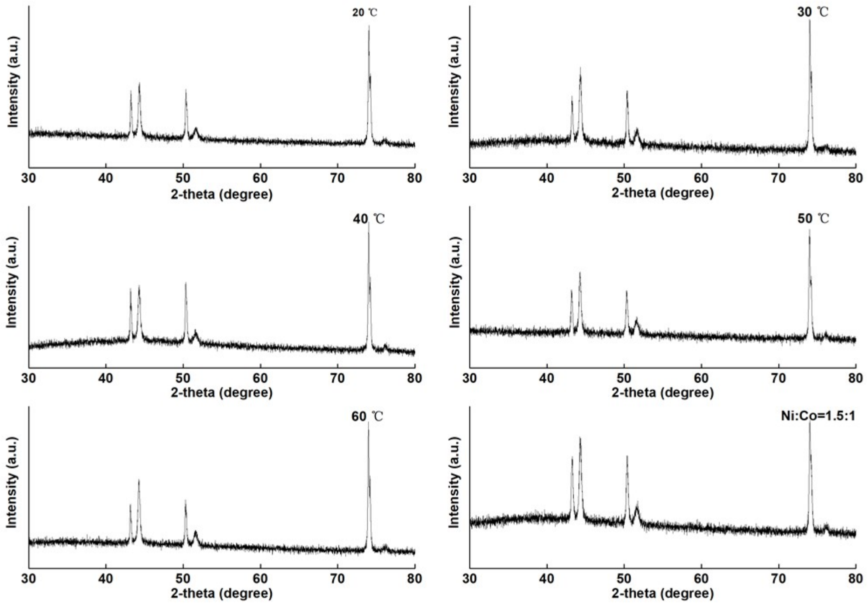

Fig. S6 shows the XRD images of the Ni:Co=1.5:1 catalyst after three LSV tests at different temperatures.

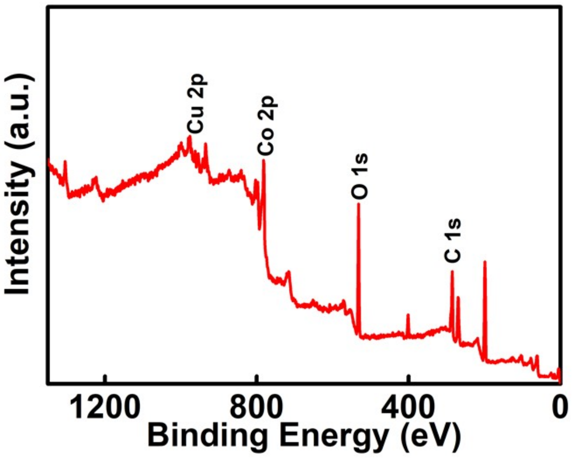

Fig. S7 The survey spectrum of amorphous Co XPS

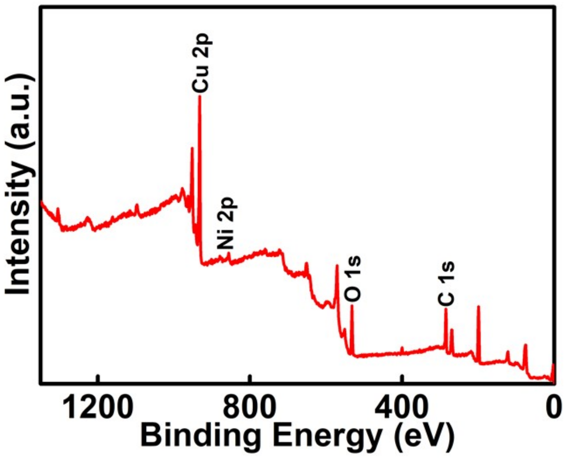

Fig. S8 The survey spectrum of Ni XPS

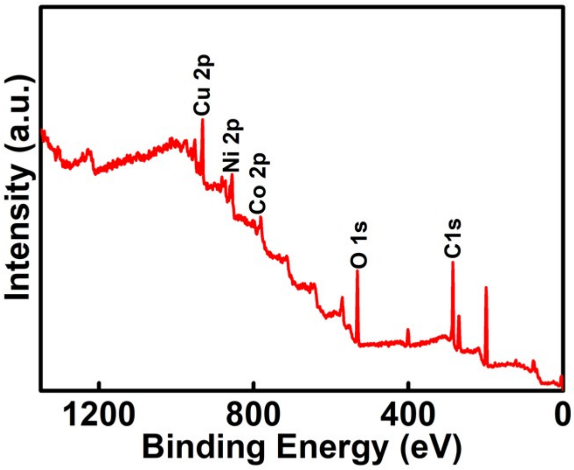

Fig. S9 The survey spectrum of amorphous Ni:Co=1.5:1 XPS

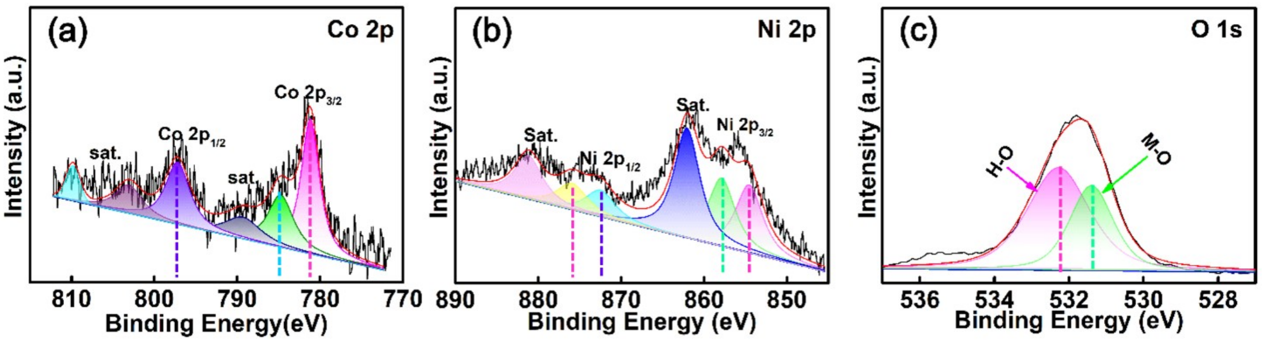

Fig. S10 a), b), c) are the XPS imaging of Co, Ni, O elements of Ni:Co=1.5:1 catalyst after 8 h HER stability test, respectively.

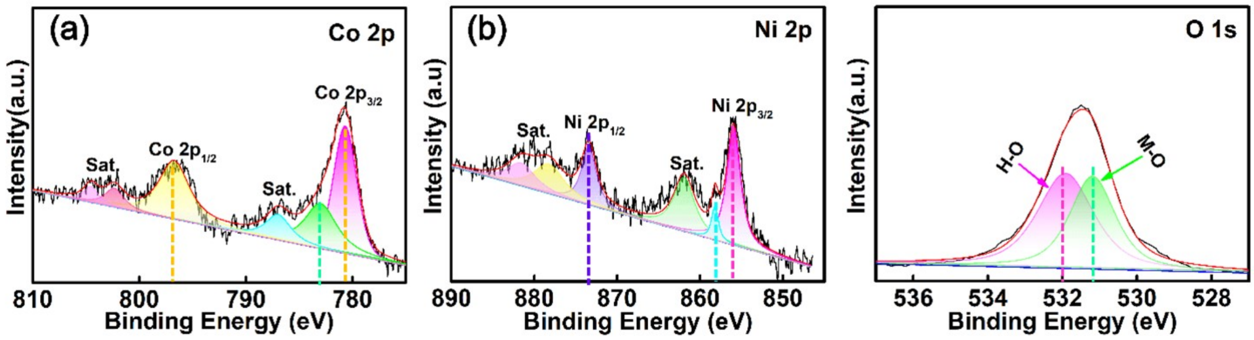

Fig. S11 a), b), c) are the XPS imaging of Co, Ni, O elements of Ni:Co=1.5:1 catalyst after 8 h OER stability test, respectively.

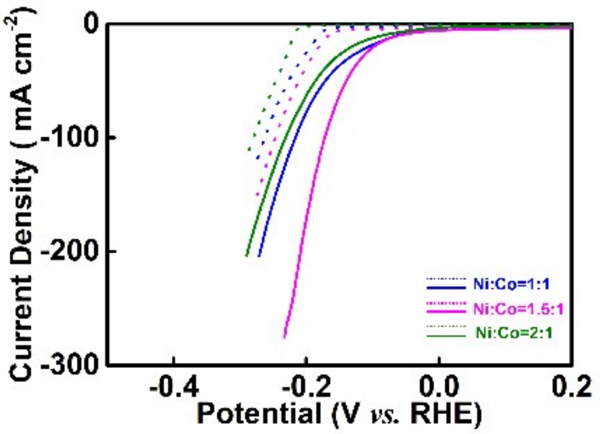

Fig. S12 HER performance of different samples in 1.0 m KOH. LSV curves of samples of Ni:Co=1:1 ; 1.5:1; and 2:1alloy, respectively. (The solid and dashed lines represent the test environment of the room with a temperature of 60 °C, respectively)

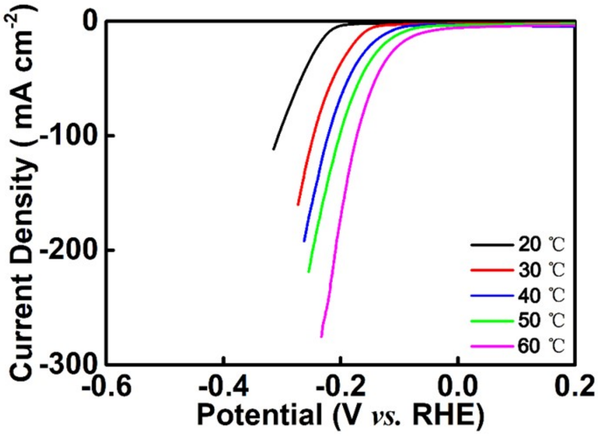

Fig. S13 HER performance of different temperatures in 1.0 m KOH. LSV curves of samples of Ni:Co= 1.5:1 at 20℃, 30℃, 40℃, 50℃ and 60℃, respectively.

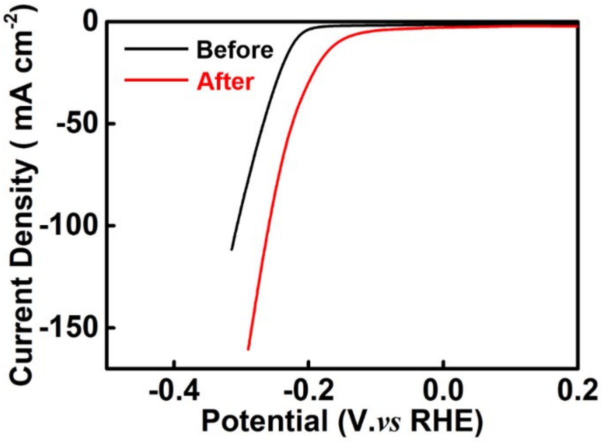

Fig. S14 HER activity of LSV curve before and after cooling of Ni:Co=1.5:1 alloy sample.

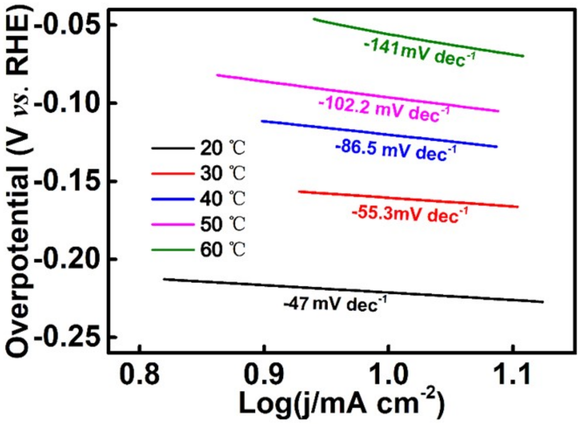

Fig. S15 HER performance in 1.0 m KOH. Tafel slope of samples of Ni:Co= 1.5:1 at 20℃, 30℃, 40℃, 50℃ and 60℃, respectively.

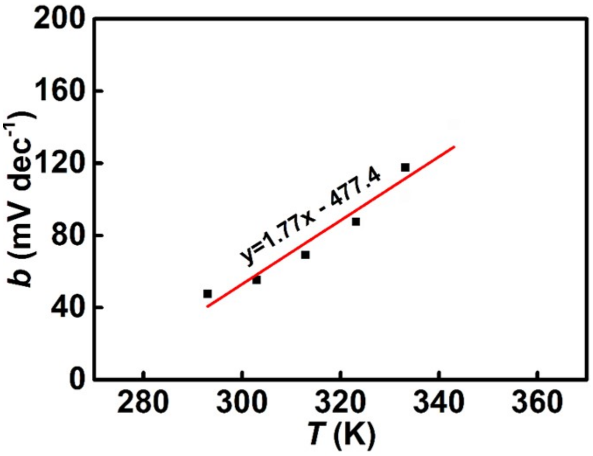

Fig. S16 The results reveal one linear relationship for the Tafel slope and for the entire set of temperatures of Ni:Co=1.5:1 sample.

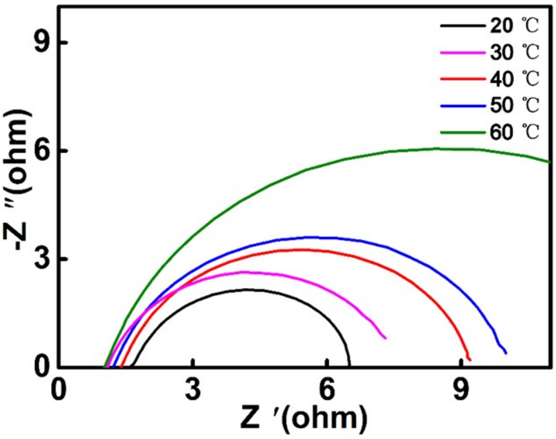

Fig. S17 HER performance in 1.0 m KOH. EIS of Ni:Co= 1.5:1 at 20℃, 30℃, 40℃, 50℃ and 60℃, respectively.

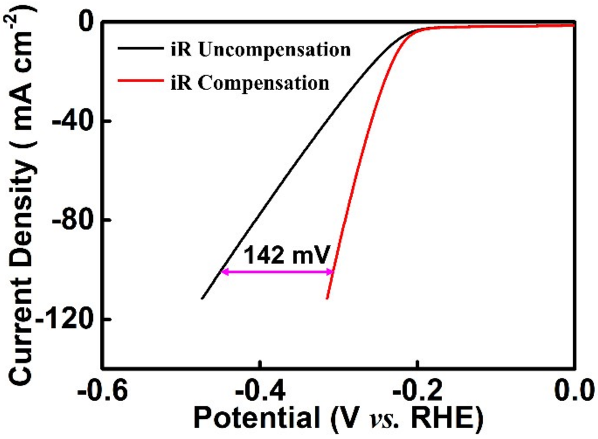

Fig. S18 HER performance in 1.0 m KOH. LSV of Ni:Co= 1.5:1 iR before and after compensation at 20℃, respectively.

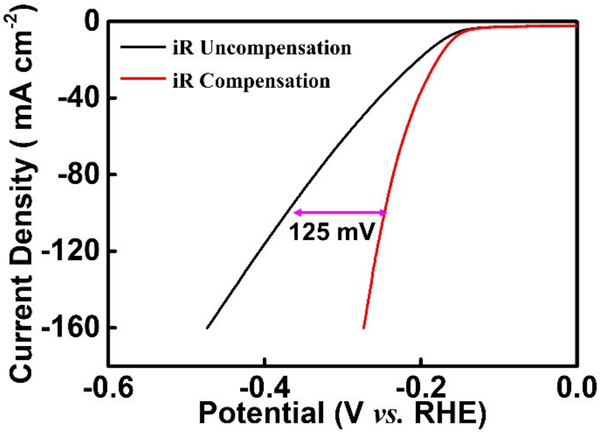

Fig. S19 HER performance in 1.0 m KOH. LSV of Ni:Co= 1.5:1 *i*R before and after compensation at 30°C, respectively.

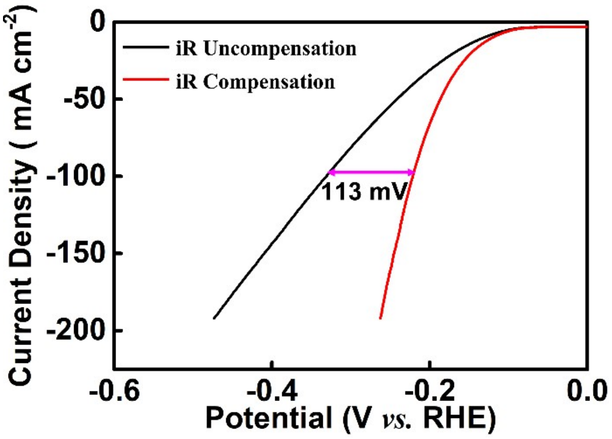

Fig. S20 HER performance in 1.0 m KOH. LSV of Ni:Co= 1.5:1 *i*R before and after compensation at 50°C, respectively.

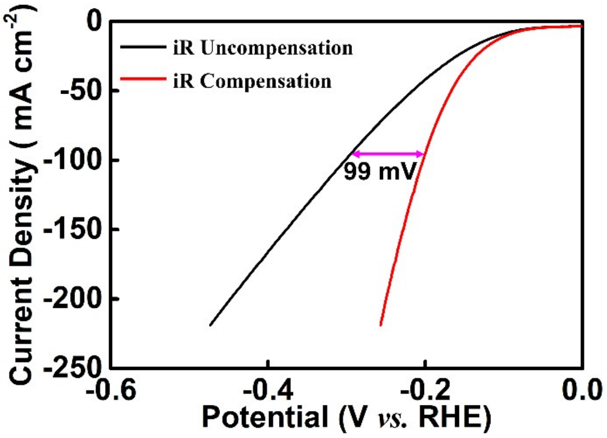

Fig. S21 HER performance in 1.0 m KOH. LSV of Ni:Co= 1.5:1 *i*R before and after compensation at 60°C, respectively.

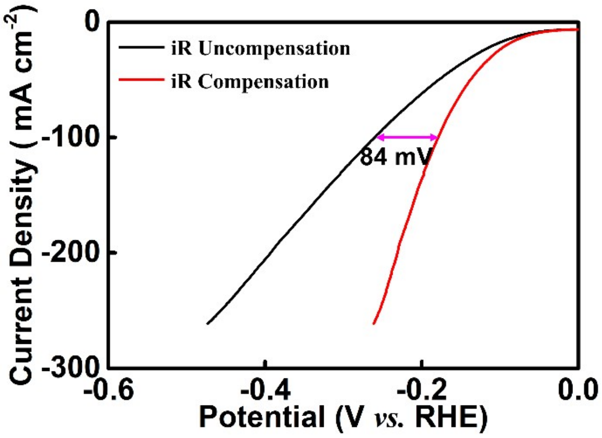

Fig. S22 HER performance in 1.0 m KOH. LSV of Ni:Co= 1.5:1 *i*R before and after compensation at 60°C, respectively.

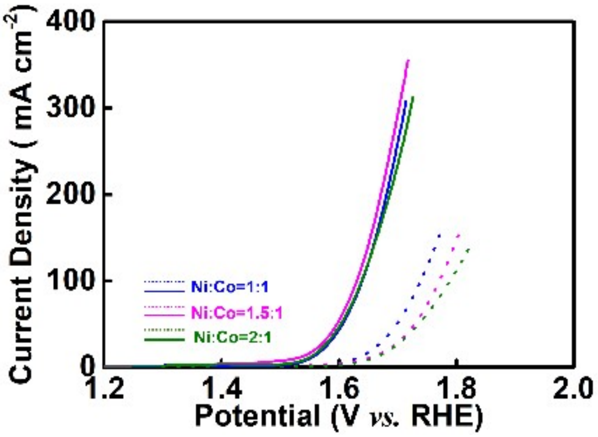

Fig. S23 OER performance of different samples in 1.0 m KOH. LSV curves of samples of Ni:Co=1:1; 1.5:1; and 2:1 alloy, respectively. (The solid and dashed lines represent the test environment of the room with a temperature of 60 ° C, respectively).

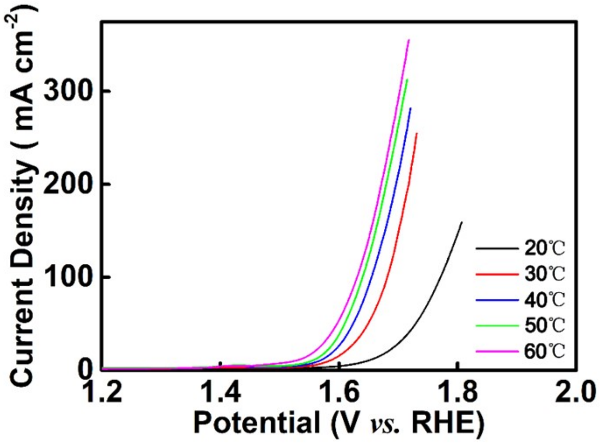

Fig. S24 OER performance of different temperatures in 1.0 m KOH. LSV curves of samples of Ni:Co= 1.5:1 at 20°C, 30°C, 40°C, 50°C and 60°C, respectively.

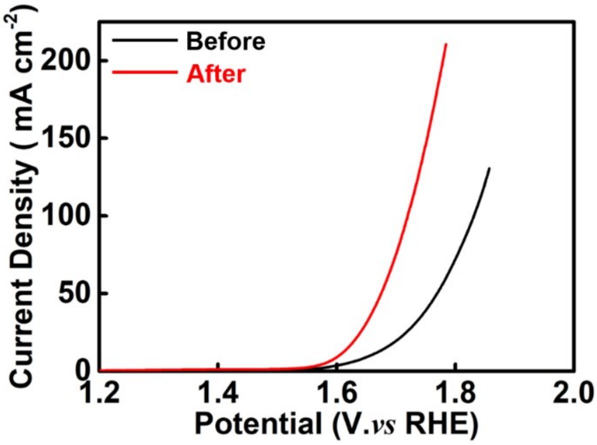

Fig. S25 OER activity of LSV curve before and after cooling of Ni:Co=1.5:1 alloy sample

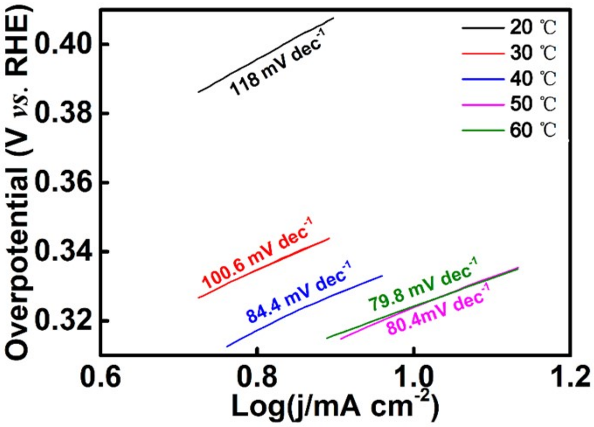

Fig. S26 OER performance in 1.0 m KOH. Tafel slope of samples of Ni:Co= 1.5:1 at 20℃, 30℃, 40℃, 50℃ and 60℃, respectively.

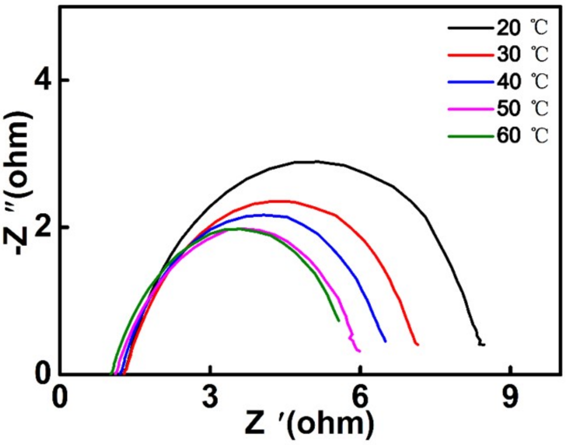

Fig. S27 OER performance in 1.0 m KOH. EIS of Ni:Co= 1.5:1 at 20℃, 30℃, 40℃, 50℃ and 60℃, respectively.

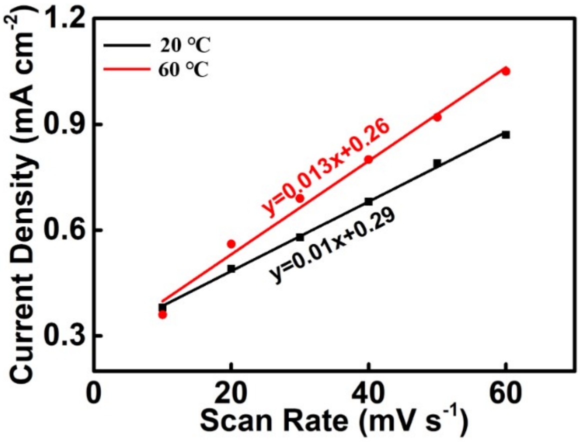

Fig. S28 The corresponding capacitive currents as a function of the scan rate of amorphous Co.

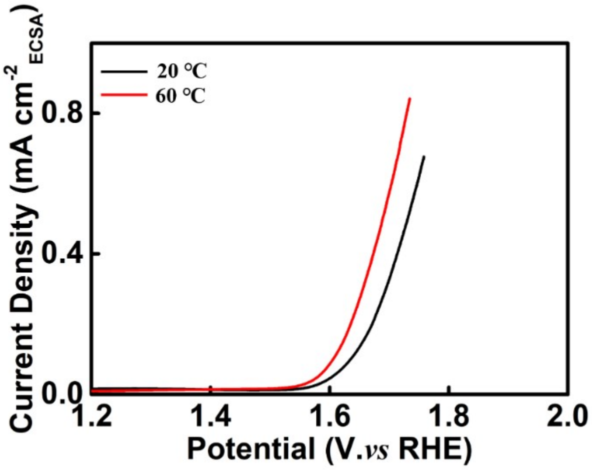

Fig. S29 ECSA-normalized LSV curves of amorphous Co.

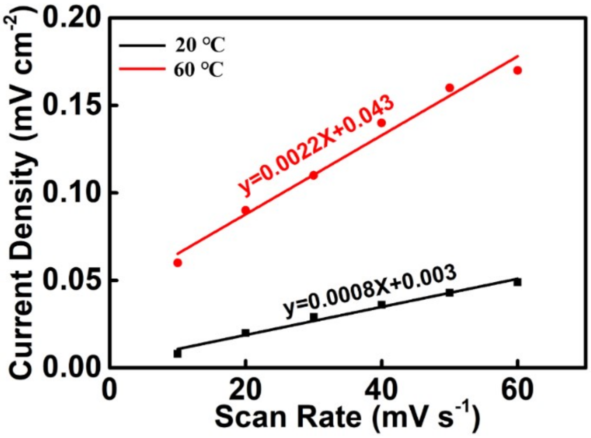

Fig. S30 The corresponding capacitive currents as a function of the scan rate of metal Ni.

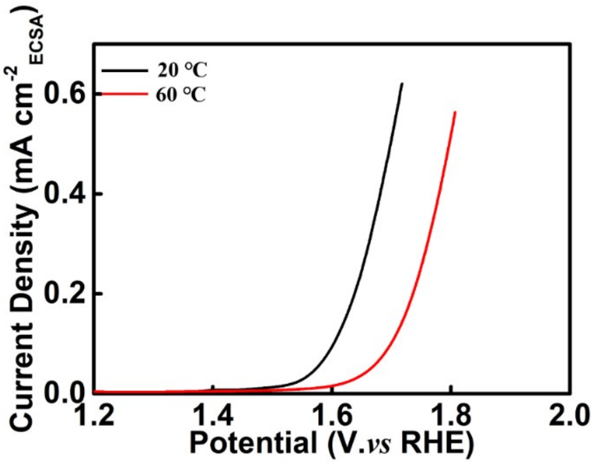

Fig. S31 ECSA-normalized LSV curves of metal Ni.

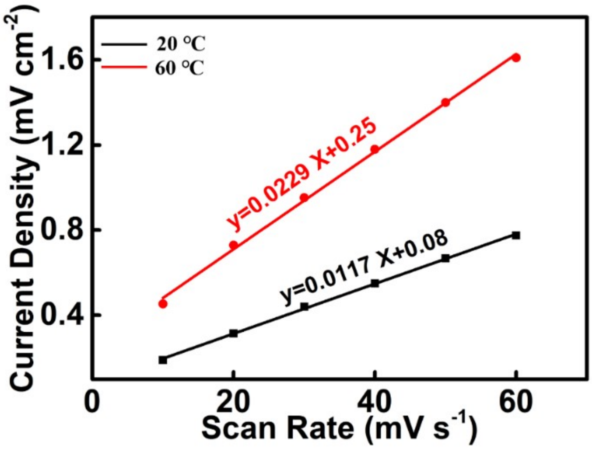

Fig. S32 The corresponding capacitive currents as a function of the scan rate of Ni:Co=1.5:1 alloy.

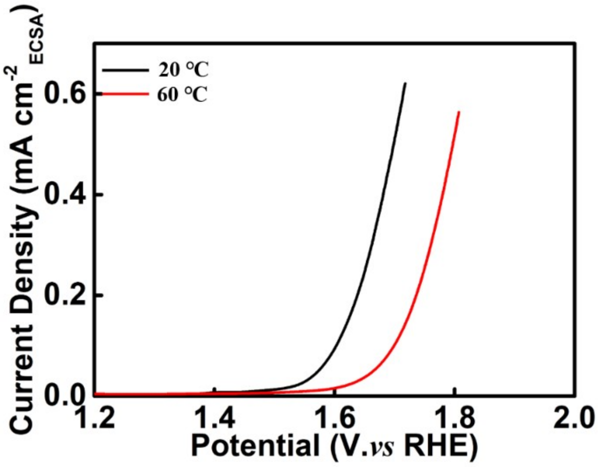

Fig. S33. ECSA-normalized LSV curves of Ni:Co=1.5:1 alloy

The optimized structures of Ni (110), Co (110) and NiCo (110) surfaces

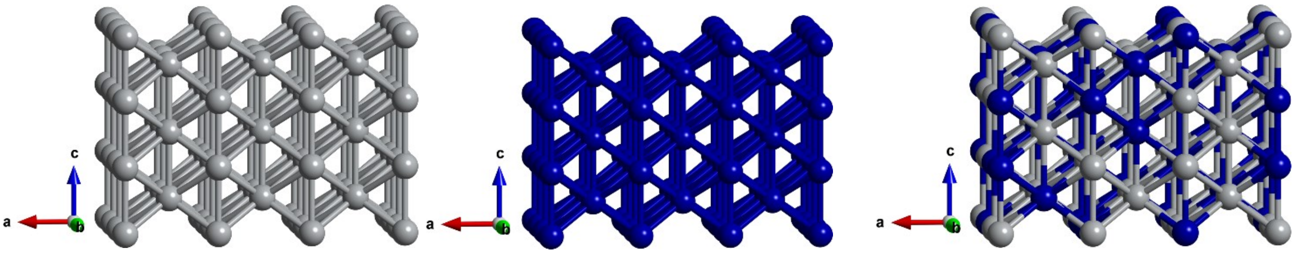

(a) Ni (110) (b) Co (110) (c) NiCo (110)

Fig. S34 The optimized structures of (a) Ni (110), (b) Co (110) and (c) NiCo (110) surfaces. Ni: grey; Co: blue.

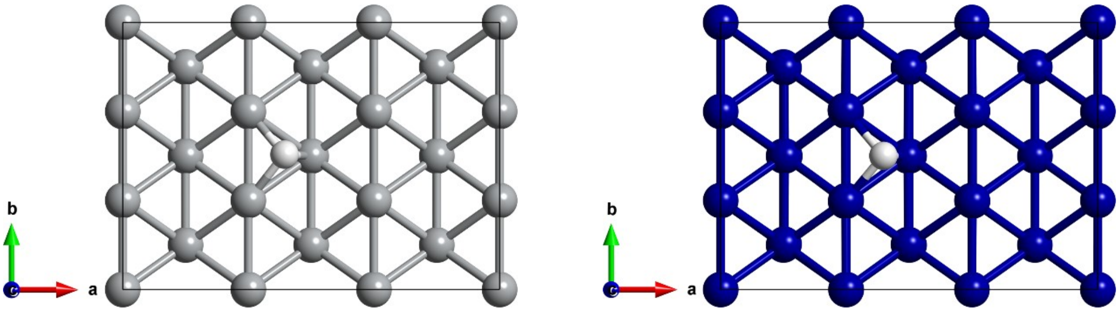

(a) H on Ni (110) (b) H on Co (110)

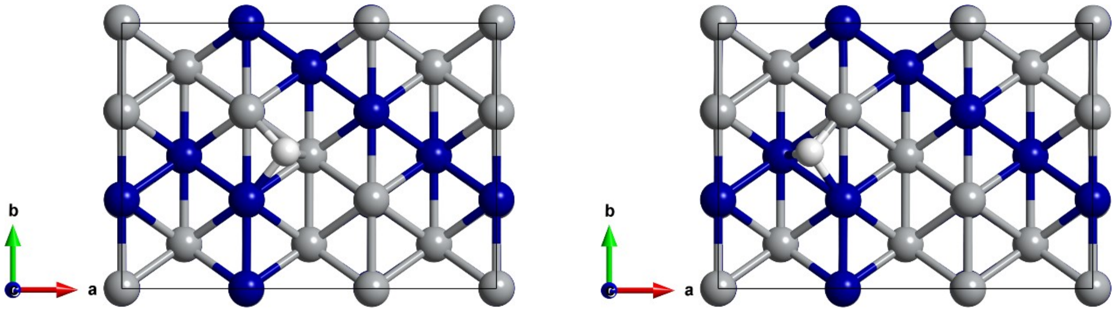

(c) H on NiCo (110) site1 (d) H on NiCo (110) site2

Fig. S35 The optimized structure of hydrogen adsorbed on Ni (110), Co (110) and NiCo (110) surfaces. Ni: greyl Co: blue; H: white.

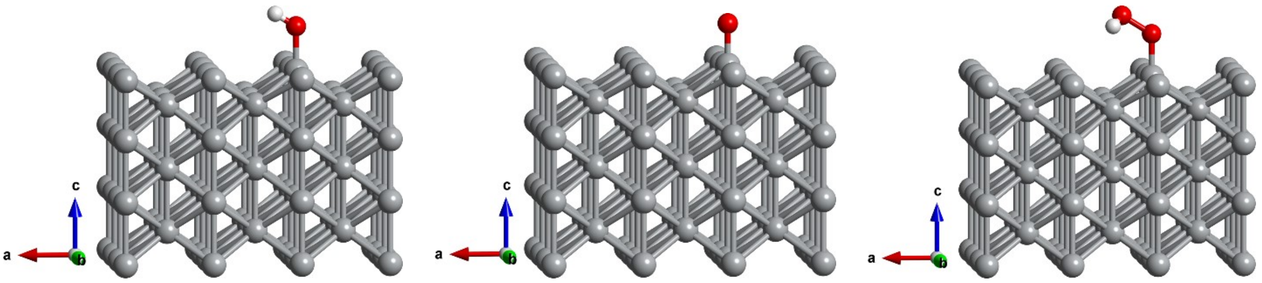

(a) OH* on Ni (110) (b) O* on Ni (110) (c) OOH* on Ni (110)

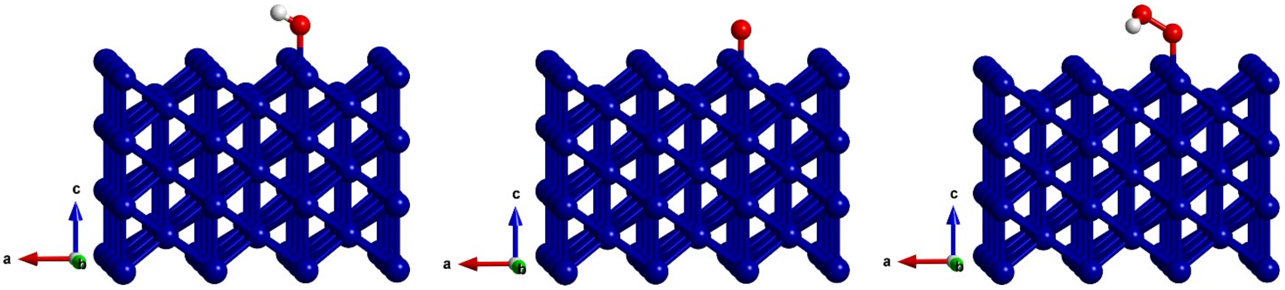

(d) OH* on Co (110) (e) O* on Co (110) (f) OOH* on Co (110)

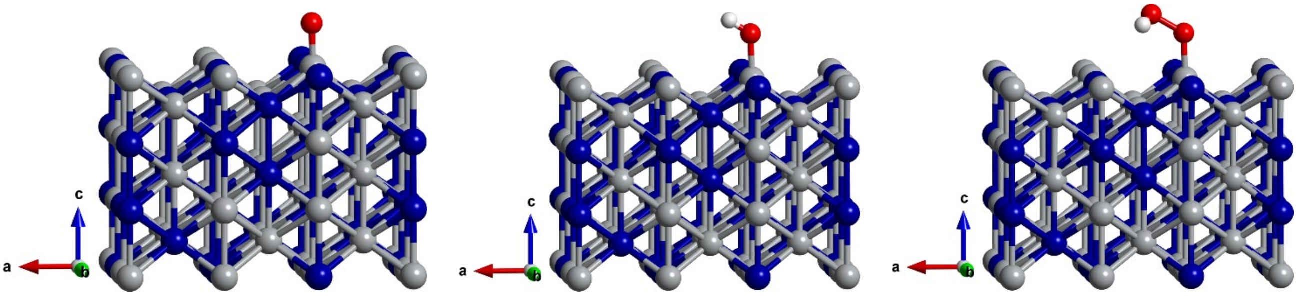

(g) OH* on NiCo (110) (h) O* on NiCo (110) (i) OOH* on NiCo (110)

Fig. S36 The optimized intermediates structures on Ni (110), Co (110) and NiCo (110). Ni: grey; Co: blue; O: red; H: white.

Table S1 ICP-OES test data results

m_o (g)	V_0 (mL)	element	C_o (mg/L)	f	C_1 (mg/L)	C_x (mg/kg)	W (%)
0.0574	100	Ni	2.18		2.180	3797.91	0.38%
0.0574	100	Co	1.39		1.390	2421.60	0.24%

Table S2 Elemental ratio and peak location of nickel to cobalt for three catalysts.

	Co 2p						Ni					
	$2p_{3/2}$		Sat.	$2p_{1/2}$		Sat.	$2p_{3/2}$		Sat.	$2p_{1/2}$		Sat.
Co	16.8%	18.6%	27.4%	16.2%	13.1%	8%						
Ni							4.4%	24.7%	36.3%	11.1%	13.9%	9.1%
Ni:Co=1.5:1	3.3%	32.6%	28.7%	17.6%	9.2%	8.5%	2.2%	20%	29.3%	16.6%	16.7%	15.2%
Ni:Co=1.5:1 post-HER	34.1%	18.6%	10.8%	20.8%	10.7%	4.9%	19.8%	19.4%	30.0%	8.4%	8.5%	13.1%
Ni:Co=1.5:1 post-OER	34.4%	21.5%	9.5%	25.7%	5.4%	3.5%	30.2%	4.3%	20.9%	16.1%	16.5%	11.9%

	Co 2p						Ni						O	
	$2p_{3/2}$		Sat.	$2p_{1/2}$		Sat.	$2p_{3/2}$		Sat.	$2p_{1/2}$		Sat.	1s	
Co	780.9	782.4	786.6	797.3	802.1	804.5							532.2	531.4
Ni							852.8	856	861.3	873.7	877.7	881.2	532.1	531.6
Ni:Co=1.5:1	777.7	781.1	785.6	797.2	801.9	803.9	852.5	855.9	861.5	873.5	878.7	882.0	532.3	531.3
Ni:Co=1.5:1 post-HER	781.2	784.8	789.3	797.2	803.1	809.8	854.5	857.9	862.1	872.5	875.9	881.2	532.3	531.4
Ni:Co=1.5:1 post-OER	780.7	783.0	787.0	796.7	802.3	804.5	855.9	858.2	861.9	873.4	878.2	881.6	531.9	531.2

The calculated HER property of Ni (110), Co (110) and NiCo (110) surfaces

Table S3 The calculated Gibbs free energy (ΔG_{H*}) of the HER process on Ni (110), Co (110) and NiCo (110) surfaces, unit: eV.

	E(surface+H)	E(surface)	$E(H_2)$	ΔE(ads)	ΔG_{H*}
Ni (110)	-346.32248896	-342.27658948	-6.8285537	-0.63162263	-0.39162263
Co (110)	-439.91571152	-435.72622089	-6.8285537	-0.77521378	-0.53521378
NiCo (110) site1	-384.41796391	-380.49960681	-6.8285537	-0.50408025	-0.26408025
NiCo (110) site2	-384.47905311	-380.49960681	-6.8285537	-0.56516945	-0.32516945

To reveal the origin of the enhanced HER activity of NiCo alloy, density functional theory (DFT) calculations were carried out. Generally, hydrogen evolution activity is closely related with the Gibbs free energy of hydrogen adsorption (ΔG_{H*}) on the surfaces of catalysts in both acid and alkaline conditions, so $|\Delta G_{H*}|$ is one of the key catalytic descriptors for theoretical prediction of HER activity, which is usually proposed to have an optimal value being close to zero [7,8]. In this context, NiCo alloy (site1) has the lowest $|\Delta G_{H*}|$ (-0.264 eV) than other site.

The calculated OER property of Ni (110), Co (110) and NiCo (110) surfaces

Table S4 The calculated intermediate energies (eV), zero-point energies (ZPE) and entropy contributions (TS) of the OER process of Ni (110), Co (110) and NiCo (110) surfaces, unit: eV.

Ni (110)	E	ZPE	TS	G
surface	-342.27658948	/	/	-342.27658948
OH*	-353.05200375	0.31635300	0.10279300	-352.83844375
O*	-348.23464404	0.05464700	0.10362600	-348.28362304
OOH*	-357.39112784	0.41842700	0.16696500	-357.13966584

Co (110)	E	ZPE	TS	G
surface	-435.72622089	/	/	-435.72622089
OH*	-446.74679873	0.31708700	0.09351100	-446.52322273
O*	-442.23376594	0.06105000	0.07187800	-442.24459394
OOH*	-450.97692459	0.39745100	0.19095000	-450.77042359

NiCo (110)	E	ZPE	TS	G
surface	-380.49960681	/	/	-380.49960681
OH*	-391.15711673	0.31390200	0.10069800	-390.94391273
O*	-386.24581646	0.05538100	0.09421900	-386.28465446
OOH*	-395.50876385	0.38842700	0.19696500	-395.31730185

Table S5 The calculated Gibbs free energy change (eV) of the OER process of Ni (110), Co (110) and NiCo (110) surfaces, unit: eV.

	Ni (110)	Co (110)	NiCo (110)
ΔG1	0.34646873	0.11132116	0.46401708
ΔG2	1.14054386	0.86435194	1.24498142
ΔG3	2.05228020	2.38249335	1.87567561
ΔG4	1.38070711	1.56183345	1.33532579

Table 6 The calculated plot energy (eV) of the OER process of Ni (110), Co (110) and NiCo (110) surfaces, unit: eV.

U=0 V	Ni (110)	Co (110)	NiCo (110)
H_2O	0	0	0
OH*	0.34646873	0.11132116	0.46401708
O*	1.48701259	0.97567310	1.70899850
OOH*	3.53929279	3.35816645	3.58467411
O_2	4.92	4.92	4.92
η^{OER}	0.82228020	1.15249335	0.64567561

过电势：η^{OER}

References：

[1] G. Kresse and J. Furthmu ̈ller, Comput.Mater.Sci., 1996, 6, 15–50.
[2] J. P. Perdew, K. Burke and M. Ernzerhof, Phys. Rev. Lett., 1996, 77, 3865–3868.
[3] P. E. Blöchl, Phys. Rev. B: Condens. Matter Mater. Phys., 1994, 50, 17953–17979.
[4] G. Kresse and D. Joubert, Phys. Rev. B: Condens. Matter Mater. Phys., 1999, 59, 1758.
[5] J. K. Nørskov, T. Bligaard, A. Logadottir, J. Kitchin, J. G. Chen, S. Pandelov, U. Stimming, J. Electrochem. Soc. 2005, 152, J23.
[6] C. Tsai, K. Chan, J. K. Nørskov and F. AbildPedersen, Catal. Sci. Technol., 2015, 5, 246–253.
[7]J. Su, Y. Yang, G. Xia, J. Chen, P. Jiang and Q. Chen, Nat. Commun., 2017, 8, 14969.
[8]P. Chen, K. Xu, S. Tao, T. Zhou, Y. Tong, H. Ding, L. Zhang, W. Chu, C. Wu and Y. Xie, Adv. Mater., 2016, 28, 7527-7532.